This is a repository copy of *Streaked extreme ultraviolet imaging of the motion of low-Z foam buffered indirectly driven intermediate and high-Z payloads*.

White Rose Research Online URL for this paper:
https://eprints.whiterose.ac.uk/id/eprint/44570/

Version: Published Version

Article:

Pasley, J. orcid.org/0000-0001-5832-8285, Nilson, P., Willingale, L. et al. (6 more authors) (2006) Streaked extreme ultraviolet imaging of the motion of low-Z foam buffered indirectly driven intermediate and high-Z payloads. Physics of Plasmas. 032702. ISSN: 1089-7674

https://doi.org/10.1063/1.2183749

Reuse
Items deposited in White Rose Research Online are protected by copyright, with all rights reserved unless indicated otherwise. They may be downloaded and/or printed for private study, or other acts as permitted by national copyright laws. The publisher or other rights holders may allow further reproduction and re-use of the full text version. This is indicated by the licence information on the White Rose Research Online record for the item.

Takedown
If you consider content in White Rose Research Online to be in breach of UK law, please notify us by emailing eprints@whiterose.ac.uk including the URL of the record and the reason for the withdrawal request.

eprints@whiterose.ac.uk
https://eprints.whiterose.ac.uk/

PHYSICS OF PLASMAS **13**, 032702 (2006)

Streaked extreme ultraviolet imaging of the motion of low-*Z* foam buffered indirectly driven intermediate and high-*Z* payloads

J. Pasley,[a] P. Nilson, L. Willingale, and M. G. Haines
Plasma Physics Group, Imperial College London, Blackett Laboratory, Prince Consort Road, London, SW7 2BZ, United Kingdom

M. Notley, M. Tolley, and D. Neely
Central Laser Facility, CLRC Rutherford Appleton Laboratory, Chilton, Didcot, Oxon, OX11 0QX, United Kingdom

W. Nazarov
University of St. Andrews, School of Chemistry, St. Andrews, KY16 9AJ, United Kingdom

O. Willi
University of Dusseldorf, Dusseldorf, Germany

(Received 6 June 2005; accepted 14 February 2006; published online 29 March 2006)

Results of experiments conducted at the Central Laser Facility (Rutherford Appleton Laboratory), illustrating the efficacy of utilizing a combination of transonic and subsonic ablation to increase the impulse delivered to an indirectly driven payload, are reported. Extreme ultraviolet imaging has been utilized to map the trajectory of the rear surface of an accelerating payload driven by a hohlraum with a peak energy-density-equivalent radiation temperature of around 130 eV. Payloads comprising an approximately 30–μm–thick solid-density plastic foil doped with chlorine, both with and without a gold flashing on the driver-facing surface, were accelerated by a combination of subsonic x-ray ablation of the rear surface of the payload and either subsonic, transonic, or supersonic ablation in a hohlraum facing low-density foam layer in intimate contact with the payload. Two different thicknesses of foam layer were incorporated in the experiment — 150 and 200 μm — in addition to a range of different foam densities from 30 to 100 mg/cc. It was observed that the maximum impulse was delivered in the case where the ablation wave propagation was approximately transonic in the foam layer. In such cases the impulse delivered to the payload was significantly greater than that achieved by direct (subsonic) ablation of the payload.
© *2006 American Institute of Physics*. [DOI: 10.1063/1.2183749]

I. INTRODUCTION

Indirect drive inertial confinement fusion (ICF) relies upon the implosion of a spherical capsule containing deuterium-tritium (DT) fuel to high densities and temperatures by the pressure exerted through the subsonic x-ray ablation of the surface of the spherical shell. This shell is composed of low-atomic number (low-*Z*) atoms (beryllium or hydrocarbon plastic) plus higher-*Z* dopants added to prevent shell and fuel preheating by nonthermal components of the drive spectra. The inclusion of such dopants reduces the drive efficiency since the albedo of the ablator is increased. Here we discuss the use of tamping to overcome this problem.

A low-*Z* foam intermediary between the drive and payload (first reported in Ref. 1) modifies the time-pressure history seen by the payload, first by passively containing the rarefaction wave, and then by actively pushing back.

When cold, the tamper material has a relatively low opacity to the hotter components of the soft x-ray drive. Consequently, the driver-facing surface of the pusher will experience radiant heating from the outset, in spite of the presence of the tamper. Because the tamper is much more transparent to radiation than the pusher, the energy density is significantly unbalanced across the tamper-pusher interface, and the pusher material expands into the low-density tamper.[2]

As time progresses the tamper will be heated to an increasing depth by a propagating heat wave driven primarily by the softer components of the x-ray drive. Once this heat wave approaches the boundary with the pusher material, three possible scenarios arise. The ablated pusher material will either be snowplowed back toward the denser regions of the pusher, remain quasistatic, or else continue to expand into the tamper. We designate these three possibilities "over tamped," "critically tamped," and "under tamped," respectively.

There are also three possible mechanisms for the heating of the tamper:[3] subsonic ionization, where a shock wave leads the heating wave; transonic ionization, where the heat wave is closely tied to the shock wave [separation <1 radiation mean free path (m.f.p.)]; and finally supersonic ionization, where the heat wave propagates sufficiently rapidly that the material does not have time to form a shock wave. In this latter case, although no shock wave will form, the material will still be accelerated somewhat by the passage of the heat

---

[a] Present address: Center for Energy Research, University of California at San Diego, 9500 Gilman Drive, La Jolla, CA 92093-0417. Electronic mail: jpasley@ucsd.edu

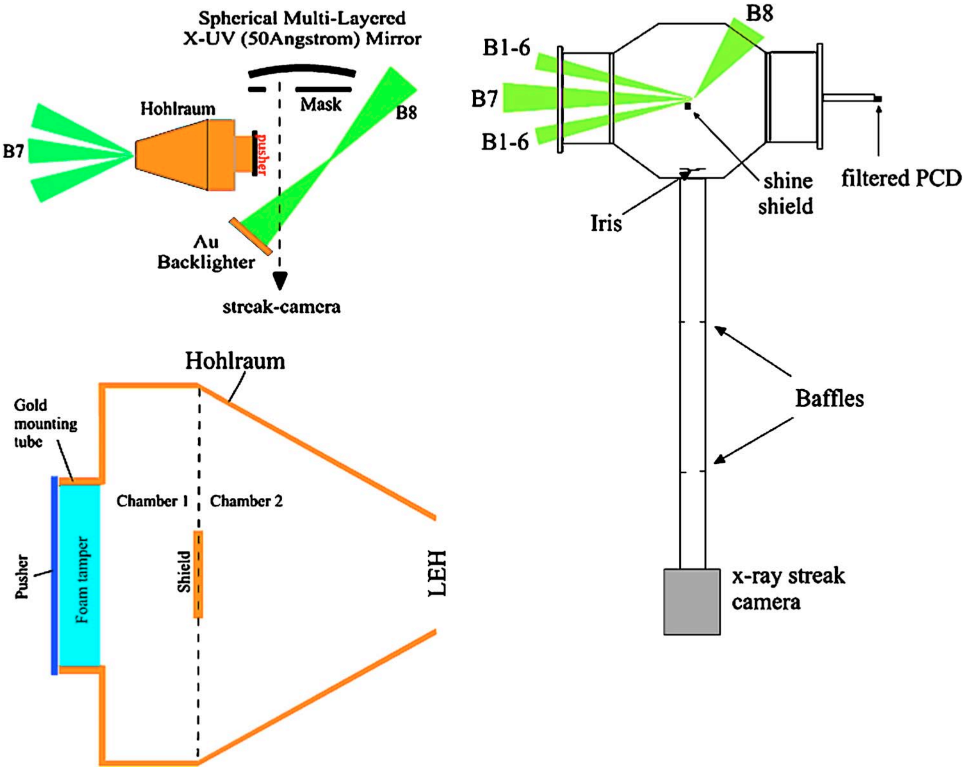

FIG. 1. (Color online) The experimental arrangement.

front – though this acceleration becomes negligible in the highly supersonic regime. In the other two cases, the ionization wave is followed immediately by a rarefaction (assuming the tamper is not itself restricted from moving.) Subsonic and supersonic ionization fronts are stable, assuming that the heated tamper material is relatively transparent to the drive (i.e., low-Z). Transonic fronts tend to collapse into the stable subsonic configuration if the drive temperature is held constant.

Each of the three types of ionization wave has a different pressure versus radiation temperature scaling associated with it.[4] In the subsonic regime, pressure goes approximately with $T^{3.5}$ (Ref. 5). Around the transonic point the scaling becomes more complicated: the pressure reaches a peak at the transonic point, then falls off. This drop in pressure is due to the disappearance of the shock wave upon entering the supersonic regime. Once the propagation becomes significantly supersonic, the scaling becomes approximately linear with temperature [$\cong nkT$ where n is the number density of particles (ions+electrons) and k is the Boltzmann constant].

In addition to the material pressure associated with the heated tamper fluid, ram pressure also acts on the pusher. Ram pressure is the pressure due to the momentum coupling between the ionization-wave-accelerated tamper material and the pusher.[6] In the subsonic case, this amounts to shock wave acceleration at a low$\rightarrow$high impedance boundary as the shock lead ionization wave reaches the pusher.[7] In the supersonic case, the rarefaction can lag significantly behind the heat front, so a weaker, yet more prolonged, impetus is conveyed.

In high-Z materials, such as may be found in the pusher, the ionization wave propagation is almost inevitably subsonic and diffusive, except in the very earliest stages of penetration.[8] This diffusive behavior results in the ablation pressure having a strongly negative time dependence, and greatly increases the time such materials take to burn through relative to their low-Z counterparts. In the experiment described herein both chlorinated plastic and gold-coated chlorinated plastic pushers were employed. Comparison with previous results for targets in which less opaque pusher material was employed shows that the acceleration of the present set of targets relied much more heavily upon the tamper pressure than was the case when more efficient subsonic ablators were employed.

Subsonic ionization is equivalent to the usual ablation mechanism that is responsible for driving the implosion of conventional indirect drive ICF fuel capsules. Transonic behavior in the acceleration of simple ICF capsules is also important; the final "shock" in the National Ignition Facility (NIF) (Ref. 9) baseline target is actually a transonic ionization wave.[4] However, the use of supersonic ionization demands the use of a tamper-pusher system in order to avoid fuel preheat.

II. EXPERIMENTAL ARRANGEMENT

The experiment was performed at the Rutherford Appleton Laboratory and driven by the Vulcan Laser System (Target Area East)[10] in February-March 2003. All beams were frequency doubled. The experimental arrangement is illustrated in Fig. 1. The major diagnostic was high magnification extreme ultraviolet (X-UV) imaging[11] of the rear (nondriver-facing) surface of the pusher. This system employed a spherical multilayer mirror, which reflected at a wavelength of 50 *Å*, imaging onto the photocathode of a high magnification $(2\times)$ x-ray streak camera. An overall magnification of ~ 140 was obtained.

The main six-cluster configuration (six-beam cone with a half angle of 13°, individual beam diameter 180 mm, $\sim$220 J infrared (IR) per beam in a 2–ns square pulse), along with a seventh beam (220-mm diam, $\sim$350 J IR in a 4-ns square pulse) propagating along the axis of the cluster, were used to heat a hohlraum. This gave a total maximum energy into the hohlraum of around 1 kJ in green, given an average conversion efficiency of approximately 56%. The eighth beam was focused onto a gold backlighter disk. The hohlraum has a two-chamber design, the object of which is to maximize the achievable radiation temperature. The six smaller diameter beams were focused onto the rearmost wall of the hohlraum, in a region of wall that takes the form of an annulus surrounding the target-package mounting hole. The larger diameter beam was focused onto a thick gold shield that partially divided the hohlraum; this division resulting in the creation of two distinct chambers within the hohlraum. This two-chamber arrangement reduced the radiation losses from chamber 1, where the target package was mounted, since a heated second chamber was located between it and the laser entrance hole (LEH). The complete hohlraum was 1.33 mm in length and 1 mm in diameter. The target package incorporated either a 150- or 200-μm-deep, 500-μm-diam, $C_{15}H_{20}O_6$ foam tamper (mounted in a 30-μm–thick gold cylinder of equal length) in contact with a 29.8(±0.2)-μm–thick C_8H_7Cl pusher, which in some cases was coated with 0.2(±0.01) μm of gold on the driver-facing surface. The foam was manufactured using a form of *in situ* polymerization.[12] For each ablator/foam length combination a pusher-only shot (i.e., without tamper) was taken, to determine the dynamics in absence of any tamping.

The 4-ns pulse length of beam seven resulted in the achievement of a remarkably flat-topped temperature profile, the peak temperature being approximately 132 eV (±5 eV) when the driver energy was optimal. In practice the driver energy fluctuated causing a similar scaled $(T_R \propto E_{laser}^{0.3})$ fluctuation of the radiation temperature. The radiation temperature pulse shape is shown in Fig. 2. The radiation pulse shape was measured with a calibrated x-ray photoconducting detector (PCD) mounted 1.5 m along the axis of rotational symmetry of the hohlraum from the target chamber center such that the surface of the diode was parallel with the plane of the target-package mounting hole. The PCD was filtered with 5.31(±0.2) μm of aluminum. Two shots were taken to confirm the radiation pulse shape. In these shots the target package and associated mounting tube were not fielded, leaving the PCD with a direct (though filtered as described) view of the hole over which the target package would ordinarily be mounted. No accurate shot-to-shot measurements of the x-ray pulse shape were made; however, a filtered silicon photodiode of $\sim 1-2$ ns time resolution was run on every shot looking at the hohlraum LEH. Since this diode integrated the x-ray signal over time periods of interest, it was used only to check for large variations in the x-ray signal such as may be associated with poor laser beam pointing. Since the target package (foam and payload) has a finite albedo to the x rays emanating from within the hohlraum, one would expect that this measurement would slightly underestimate the radiation temperatures achieved with the target package in place. The albedo of the target package is sufficiently low; however, that the difference is expected to be no more than 4.5 eV and nominally around 3.4 eV. These calculations were made using HYADES Pro Plus one–dimensional (1D) radiation-hydrodynamics simulations[13] to estimate the time-dependent albedo, based upon SESAME opacities. The results were then incorporated into a simple view factor/radiosity solver. The reader may speculate that the bare, gold flashed payload may cause a greater effect; however, since this gold surface is thin and located 150 μm away from the plane of the outermost rim of the mounting hole, whilst the rear surface of the plastic foam is plane parallel with this rim, this is not the case. Otherwise, the PCD measurement is robust; neither the PCD nor the target package has an unimpeded line of sight to any of the laser absorption point hot spots.

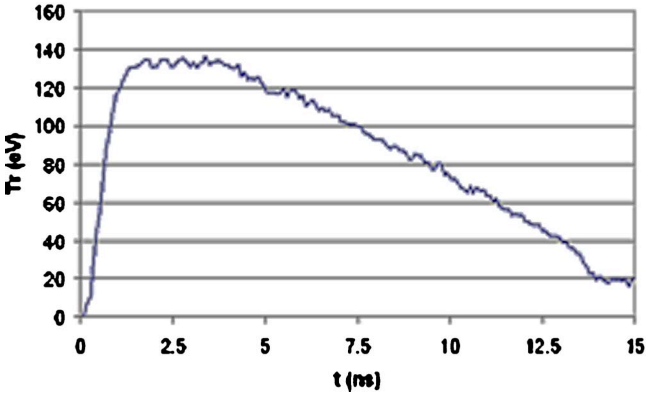

FIG. 2. The temporal profile of the x-ray drive as measured by a filtered PCD viewing the mounting hole over which a target package would ordinarily be mounted.

The use of a relatively hard (50-*Å*) X-UV backlighter allowed probing of density contours close to solid density. Although the pusher is 500 μm in diameter and is being viewed edge on by the diagnostic, only the central region of the pusher is imaged. This is achievable since, once in motion, the pusher is bowed away from the driver due to edge-loss effects in both the tamper and the pusher itself. Since the bowing is a two–dimensional (2D) effect it is has not been possible to accurately establish its extent, due to the lack of availability of a suitably flexible proven 2D-radiation-hydrodynamics simulation code. However, 2D simulations have shown that the imaged density contours will lie around 0.06 g/cc early in time, moving to around 0.16 g/cc later in time, when the bowing is more pronounced. The X-UV imaging system incorporated a spherical chromium-carbon multilayer mirror with a reflectivity of approximately 7%–10% at 50 *Å* for zero-degree incidence. The radius of curvature was 100 mm and the diameter 40 mm. Only a small ($\sim$1 cm^2) circular region of mirror was utilized in each shot, the remainder of the mirror being protected by a thick aluminum shield behind which the mirror could be rotated to

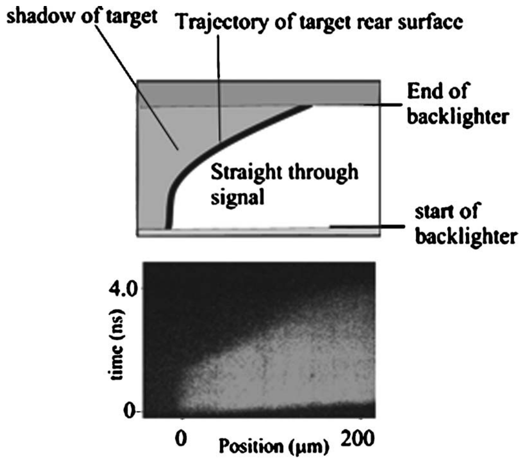

FIG. 3. A typical radiograph (bottom) with key (top). This radiograph is for a target comprising a 200-μm-deep, 70 mg/cc tamper. There is no gold flashing on the surface of the pusher.

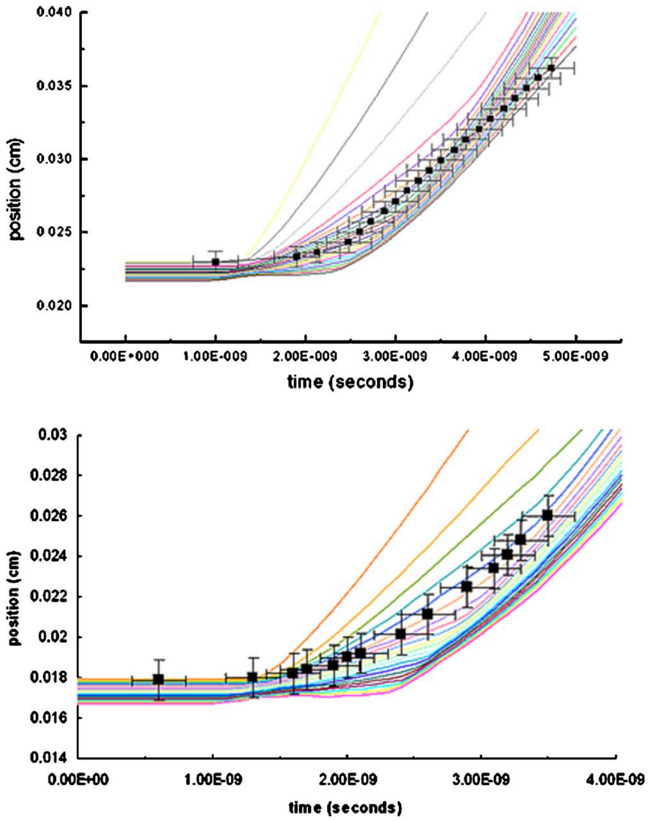

FIG. 4. (Color online) A comparison of HYADES simulation results for the rearmost half of the payload with the experimental data. Top: Data from a target comprising a 200-μm–deep, 70 mg/cc tamper is illustrated (radiograph shown in Fig. 3). Bottom: Data from a target comprising a 150-μm–deep, 100 mg/cc tamper is illustrated. There is no gold flashing on the surface of pusher in either case. Experimental data is marked with ■. Simulation data (continuous lines) is shown for the 20 Lagrangian fluid cells comprising the rearmost half of the payload.

expose a fresh surface for each shot. The exposed mirror surface was compromised on every shot, although it is not known whether this damage was caused by either x ray or scattered laser photons, or a combination of both. The shadow of the rear surface of the pusher was imaged onto the photocathode of a streak camera situated at the end of a long evacuated tube such that the magnification was about 70. A cesium iodide photocathode was employed in a high magnification Kentech camera giving an overall magnification of around 140. A small light block was employed between the target and the camera. The imaging axis was set such that the signal was sent around these various obstructions (target, backlighter, and light block); this required using the multilayer mirror slightly away from its intended zero-degree axis (by approximately half a degree); the signal strength was not unduly affected however.

III. RESULTS AND ANALYSIS

A sample radiograph is shown in Fig. 3. The trajectory of the pusher rear surface can clearly be seen. A radiograph of two 26(±0.2) μm copper wires separated by 140(±5) μm was also taken to experimentally ascertain the system magnification and resolution. The resolution was found to be approximately 4 μm or approximately 140 ps in the temporal direction.

From these radiographs the trajectory of the imaged density contour was calculated using a locus of points of constant areal density, as shown in Fig. 4. The horizontal error bars are totally systematic from uncertainty in the pulse timing. The vertical error bars are a combination of random; in locating each point ($\sim\pm 4$ μm), and systematic from the uncertain bowing of the flyer plate that determines the relation between areal and volume density; we have set the starting point on the innermost isochor of the simulation; this relation changes during the shot, as described earlier, but that is a small additional systematic effect ($\sim\pm 3\mu$m). Figure 4 also shows the calculated trajectory of these targets; we have plotted the trajectories of the rearmost Lagrangian fluid cells as determined by HYADES simulations. After the first couple of nanoseconds of flight, the pusher's rear surface ceases accelerating and proceeds at a relatively constant velocity. Since the pushers were all initially of the same mass, this final velocity serves as a measure of the relative coupling efficiency. Figure 5 illustrates the final velocities achieved in all the shots for which the streaked trajectory data was produced. The error bars in this graph reflect the random uncertainties in the data shown in Fig. 4. With the exception of the error associated with the bowing, the systematic errors have no impact on the slope measurement. Increased bowing gives a small systematic underestimate in the velocity, which is expected to be similar for every target.

In every case, the results show that the final velocity peaks in the targets in which the pushers were tamped with material in which ionization wave propagation would be expected to be either transonic or slightly supersonic. Analysis of the HYADES simulation output referred to above (which was performed for all of the targets successfully fielded) also supported this finding; however, the match in final velocity was rather poor. Similar discrepancies have been observed previously, for instance, in the MEDUSA modeling performed by Willi *et al.* in Ref. 14 (with which the present author was also involved). It is thought that these codes have difficulty in modeling transonic behavior due to sensitivity of

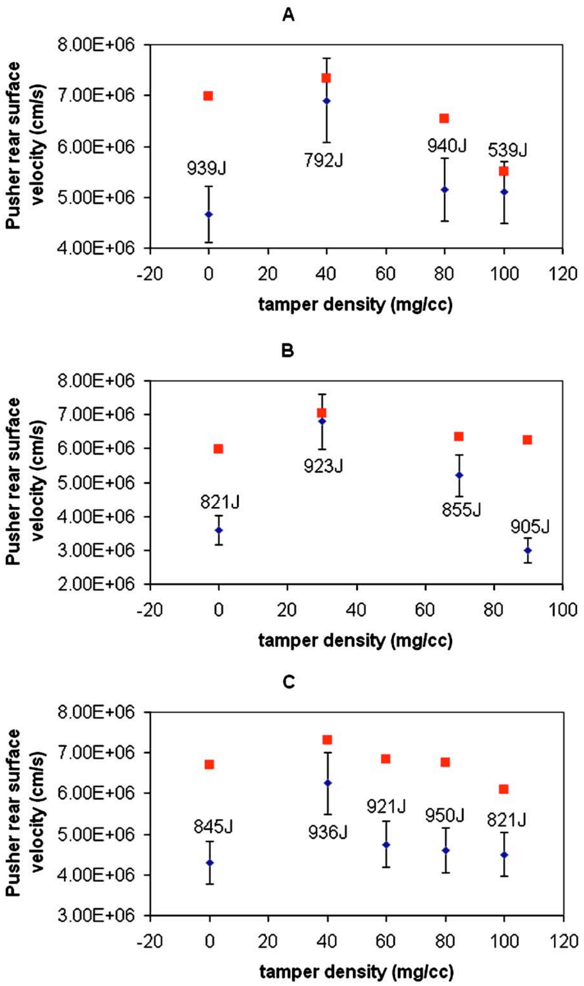

FIG. 5. Final velocity of pusher rear surface. (a) 150-μm length, no gold flash. (b) 200-μm length, no gold flash. (c) 150-μm length, gold-flashed pusher. Behavior is increasingly subsonic toward the right-hand side. HYADES results at corresponding points in the trajectory are indicated by ■.

such phenomena to the opacity and EOS models employed.

According to the analysis performed by Steve Hatchett of the Lawrence Livermore National Laboratory the critical drive temperature for transonic propagation in a given material is given by $T_{R,crit}=(4\rho_0/\sigma)^{2/5}(R/\mu)^{3/5}$, where $\mu=A/Z+1$ for the material in question, σ is the Stefan-Boltzmann constant, and R is the molar gas constant. Note that the geometry of the target dictates that the radiation field energy density should be described by a somewhat lower T_R than that shown in Fig. 2; this can be seen by contemplating the bare foil targets in which there is clearly a less-than-unity view factor between the payload and the opening to the hohlraum. Simple view factor calculations have been employed to correct for such effects in both the drive applied in the simulation and the determination of the critical density for transonic behavior. The effective T_R employed is approximately 110 eV. As expected, the effects of the tamping are most dramatic in the targets where the tamper was thick or the pusher was coated with gold. In these targets the contribution of subsonic ablation at the surface is reduced. In the first instance, due to increased filtering by the thicker tamper, and in the second case, as a result of the significantly impaired ablative acceleration consequent upon the use of a high-Z material at the driver-facing surface of the pusher. In gold, for instance, the ablation pressure scales as $P=5T^{2.67}t^{-0.46}$ at temperatures around 100–200 eV (Ref. 6), where temperature is in heV (hundreds of eV) and t is in ns.

IV. CONCLUSIONS

In the experiment described above, in which a solid plastic pusher, tamped by a low density foam, was driven by the soft x rays emanating from a laser-driven hohlraum, the combination of material pressure, ram pressure, and subsonic ablation of the pusher has combined to deliver a significantly greater impulse to the pusher than subsonic ablation alone. Comparison with previous results by Willi *et al.*, on the Phébus laser system in 1999 (Ref. 14), reveals a similarity in the optimal behavior observed around the transonic point, but also some differences. The general reduction in velocity observed in this experiment is due to a combination of the use of less effective ablator materials (the Phébus targets were doped with only 2.3% bromine by atom density, as compared to the 6.3% chlorine encountered here) and thicker ablators. Tamping is also seen to be more generally effective here than in the Phébus shots where tamped targets only outperformed their untamped counterparts in cases in which the tamper density was optimal. Again this can be explained by considering that in the Phébus experiments the ablation process at the solid surface was more important to the overall dynamics than it was here.

To summarize, it has been demonstrated that the application of tamping is particularly effective in the case of ablators that incorporate significant quantities of intermediate-Z or high-Z material. The optimization of a tamper by the selection of a tamper density in which transonic or marginally supersonic behavior may be expected has once more been confirmed.

In the context of ICF this is an interesting technique that may allow for the more efficient use of ablators that are required to contain higher-Z atomic species in order to control radiative preheat. The technique may be particularly appropriate to double-shell capsules since these are not constrained to the same extent, in terms of the time-pressure history that may be employed to drive them, as their single-shelled counterparts. The application of tamping to single-shell capsules is more problematic since tamping tends to lead to the generation of strong shocks that are undesirable where control of entropic heating is paramount.

ACKNOWLEDGMENT

We would like to acknowledge the support of the staff of the Central Laser Facility at the Rutherford Appleton Laboratory.

[1] T. D. Shepard, O. L. Landen, J. D. Lindl, M. D. Rosen, and L. J. Suter, Bull. Am. Phys. Soc. **41**, 1422 (1996).
[2] J. Edwards, S. G. Glendinning, L. J. Suter, B. A. Remington, O. Landen, R. E. Turner, T. J. Shepard, B. Lasinski, K. Budil, H. Robey, J. Kane, H. Louis, R. Wallace, P. Graham, M. Dunne, and B. R. Thomas, Phys. Plasmas **7**(5), 2099 (2000).
[3] S. Hatchett (private communication).

[4] S. Haan (private communication).
[5] J. Lindl, Phys. Plasmas **2**(11), 3933 (1995).
[6] M. Dunne (private communication).
[7] M. Rosen and J. Hammer, Phys. Rev. E **72**, 056403 (2005).
[8] D. Batani, A. Balducci, W. Nazarov, Th. Löwer, T. Hall, M. Koenig, B. Faral, A. Benuzzi, and M. Temporal, Phys. Rev. E **63**, 4 (2001).
[9] R. D. Petrasso, C. K. Li, M. D. Cable, S. M. Pollaine, S. W. Haan, T. P. Bernat, J. D. Kilkenny, S. Cremer, J. P. Knauer, C. P. Verdon, and R. L. Kremens, Phys. Rev. Lett. **77**, 2718 (1996).
[10] C. N. Danson, L. J. Barzanti, C. B. Edwards, S. A. Edwards, C. N. Harrison, C. J. Mistry, D. Neely, P. A. Norreys, D. A. Pepler, D. A. Rodkiss, I. N. Ross, W. T. Toner, T. B. Winstone, F. N. Walsh, and R. W. Wyatt, Proc. SPIE **2633**, 316 (1995).
[11] J. Edwards, M. Dunne, R. Taylor, O. Willi, C. A. Back, and S. J. Rose, Phys. Rev. Lett. **71**(21), 3477 (1993).
[12] J. Falconer, W. Nazarov, and C. J. Horsfield, J. Vac. Sci. Technol. A **13**, 1941 (1995).
[13] HYADES is a commercial product of Cascade Applied Sciences Incorporated, 6325 Trevarton Drive, Longmont, CO 80503. (Electronic mail: larsen@casinc. com).
[14] O. Willi, J. Pasley, A. Iwase, W. Nazarov, and S. J. Rose, Proceedings of Invited Papers, 1st Inertial Fusion Sciences and Applications, Bordeaux, 1999, edited by Ch. Labaune, W. J. Hogan, and K. A. Tanaka (Elsevier, Paris, 2000), p. 122.